Available online at www.sciencedirect.com
ScienceDirect
Journal of Power Sources 174 (2007) 1188–1192
JOURNAL OF POWER SOURCES
www.elsevier.com/locate/jpowsour

Short communication

New structural approach of lithium intercalation using Raman spectroscopy

R. Baddour-Hadjean *, J.P. Pereira-Ramos

Institut de Chimie et des Matériaux Paris-Est, CNRS-UMR 7182, Groupe d'Electrochimie et Spectroscopie des Matériaux, 2-8 rue Henri Dunant, 94320 Thiais, France

Available online 30 June 2007

Abstract

In this paper, some of our recent research work about applications of Raman microspectrometry for the study of lithium insertion compounds is presented. The examples developed include (i) the $Li_xV_2O_5$ system produced either from chemical or electrochemical processes, from bulk powder and thin films electrodes; (ii) the Li/TiO_2 anatase system investigated as a composite electrode. New spectroscopic data on both systems are presented, owed to a careful experimental method and a thorough theoretical analysis. This approach allows relevant information to be provided on some aspects of the electrochemical behaviour exhibited by these electrode materials.

Keywords: Raman microspectrometry; Lithium insertion compound; TiO_2 anatase; V_2O_5

1. Introduction

Transition metal oxides constitute a large family of materials with three- or bi-dimensional crystal networks particularly well suited to accommodate foreign species in their tunnel or interlayer space. This property makes most of these compounds very attractive as negative or positive electrode materials for rechargeable lithium batteries. Even when some of them can accommodate considerable amount of Li ions, the charge–discharge processes are often accompanied by structural changes of the host lattice. The characterization of these structural transformations is of utmost importance to elucidate some crucial aspects of the electrochemical behaviour, in particular the loss of reversibility and the capacity fade upon repeated cycling. In that sense, a picture of the microscopic pattern seems to be one of the key issues by providing data which are complementary to that of obtained by X-ray diffraction. Raman spectroscopy seems to be quite promising for this purpose since a determination of frequencies of normal vibrations constitutes a very sensitive tool to detect the local structure variations. However, very few studies are devoted to the Raman features of lithiated transition metal oxides. This is probably due to the lack of reference spectra for the different phases which are formed during the discharge of the cell, a careful examination of results published earlier by different authors showing discordance regarding their Raman spectra.

In this paper, representative results will be reported in the Li/V_2O_5 and Li/TiO_2 anatase systems. A first part is aimed to establish a Raman fingerprint of the α-, ε-, δ- and γ-phases in the $Li_xV_2O_5$ system from chemically lithiated powders. Indeed, such reference spectra are difficult to be obtained reliably from the cathodic material, the presence of a Li concentration gradient within the particles under study inducing the coexistence of several phases for each average x value. A second part is devoted to the study of a real electrochemical system using *in situ* Raman microspectrometry, which allows to follow the structural changes in V_2O_5 thin films during discharge–charge processes. Finally, we report the study of the Li/TiO_2 system, which illustrates the great interest of lattice dynamics simulation to perform a quantitative analysis of the Raman features. This theoretical approach allows to interpret the whole Raman spectra of lithiated phases on the basis of their structural characteristics, providing then interesting information on some aspects of the Li insertion–extraction mechanism.

2. Experimental

Low temperature ε-$Li_{0.52}V_2O_5$ and δ-LiV_2O_5 phases have been obtained by chemical lithiation through soft chemistry reactions according to the experimental procedure described in

* Corresponding author.
E-mail address: baddour@glvt-cnrs.fr (R. Baddour-Hadjean).

0378-7753/$ – see front matter © 2007 Elsevier B.V. All rights reserved.
doi:10.1016/j.jpowsour.2007.06.177

Ref. [1]. γ-LiV_2O_5 phase was prepared by heating at 250 °C in air the chemically prepared δ-LiV_2O_5. V_2O_5 thin films have been prepared by dc sputtering according to the experimental conditions reported in Ref. [2]. TiO_2 anatase has been prepared through the conventional sol–gel process [3]. Lithiated samples were obtained by the electrochemical route using a lithium salt in organic electrolyte. The Raman spectra were recorded at room temperature using micro-Raman system described in Ref. [3]. Lattice dynamics simulations were performed using the valence force field (VFF) potential model for the oxide lattice, which has been supplemented by the Li–O, Li–Ti and Li–Li potentials according to the theoretical approach described in Ref. [3].

3. Results and discussion

3.1. The Li/V_2O_5 system: reference Raman spectra

Depending on the amount of lithium (x) intercalated in V_2O_5, several structural modifications have been reported [1,4–8]. Considering the bulk material, the α-, ε- and δ-$Li_xV_2O_5$ were identified in the $0 < x \leq 1$ composition range. The α-$Li_xV_2O_5$ phase occurs with $x < 0.1$. The ε-phase exists in the range $0.3 < x < 0.7$ and the pure δ-phase is found for x between 0.9 and 1. All these phase transitions are fully reversible in this composition range. For lithium contents larger than 1, the δ-phase is transformed into the γ-one via an irreversible reconstruction mechanism [4]. The γ-phase structure remains stable even after deintercalation of all Li atoms, leading to a new metastable γ′ variety of V_2O_5 [9].

The local environment of the vanadium atom in V_2O_5 leads to the existence of four types of vanadium–oxygen bonds [10] (V–O bond lengths d_1–d_4 vary from 1.58 Å to 2.02 Å): short and strong V=O1 bonds oriented along the c axis ($d_1 = 1.5848$ Å), bridge V–O3 bonds ($d_2 = 1.7798$ Å), and inter-chain V–O2 bonds ($d_3 = 1.8777$ Å and $d_4 = 2.0206$ Å).

Chemically prepared ε-$Li_{0.52}V_2O_5$ and δ-LiV_2O_5 phases are typical of well-crystallized samples. Fig. 1 shows the Raman spectra of α-V_2O_5 (space group *Pmmn* or D_{2h}), ε-$Li_{0.52}V_2O_5$ (space group *Pmmn* or D_{2h}) and δ-LiV_2O_5 (space group *Amma* or D_{2h}^{17}) powders. Polarized Raman spectra for V_2O_5 crystal have been previously studied [11]. The Raman features of crystalline V_2O_5 are composed of nine peaks at about 145 cm^{-1}, 196 cm^{-1}, 283 cm^{-1}, 304 cm^{-1}, 404 cm^{-1}, 480 cm^{-1}, 526 cm^{-1}, 697 cm^{-1} and 994 cm^{-1} (Fig. 1a). Most of the low-frequency modes can be described in terms of external modes of V_2O_5 units. They have been derived from relative motions of two V_2O_5 units belonging to the unit cell, two of them generating translational modes at 145 cm^{-1} and 196 cm^{-1}. Internal modes on the other hand, which are observed in the medium and high-frequency region, can be described in terms of O–V–O, V–O–V bending modes and V–O stretching modes. The band at 994 cm^{-1} is assigned to the stretching vibration mode of the shortest V–O_1 bond directed along the c axis. The strong intensity of the translational mode located at 145 cm^{-1} reflects the long-range order in the plane of the V_2O_5 sheets.

The Raman spectrum recorded for ε-$Li_{0.52}V_2O_5$ (Fig. 1b) exhibits several spectroscopic changes: the intensity of the translational mode is strongly quenched and its wavenumber is shifted from 145 cm^{-1} to 154 cm^{-1}. Several modes in the 200–700 cm^{-1} range are also shifted towards higher wavenumber: 196–218 cm^{-1}, 404–420 cm^{-1}, 480–486 cm^{-1}, 526–535 cm^{-1} and 697–703 cm^{-1}. Conversely, the V=O stretching mode along the c axis decreases in frequency from 994 cm^{-1} to 983 cm^{-1}. This shift in frequency has been shown to be consistent with the lengthening of the V=O bond from 1.58 Å for the α-phase to 1.6 Å for the ε-phase [12].

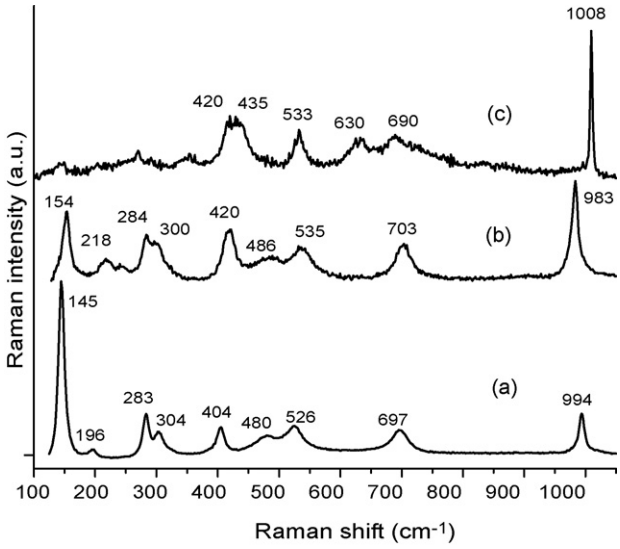

Fig. 1. Raman spectra obtained for α-V_2O_5 (a) ε-$Li_{0.52}V_2O_5$ (b) and δ-LiV_2O_5 (c).

The Raman spectrum of δ-LiV_2O_5 (Fig. 1c) can also be compared with that of α-V_2O_5 shown in Fig. 1a. Low intensity of the bands in the low-frequency part of Raman spectrum lines as well as the broadening of the bands overall the spectrum of the δ-phase indicates that this phase is less ordered than the α- and ε-lattices. It is seen also that the same sole line, corresponding to the V=O stretching mode along the c axis, dominates in the high-frequency part of both spectra. In the δ-phase spectrum, this line is narrow and shifted up to 1008 cm^{-1} with respect to 994 cm^{-1} typical for the α-phase. This line can serve as a spectral fingerprint of the δ-phase. Other marked distinctions of Raman spectrum of this phase are the presence of the peak at 630 cm^{-1} and the disappearance of the peak at 480 cm^{-1}.

The Raman features of the δ-phase reflect the particularity of this structure. The O1–O1 distances in the δ-phase (2.77 Å) are markedly shorter than in the α- and ε-phases (3 Å). The relatively high wavenumber of the V=O stretching mode is probably a spectroscopic manifestation of the steric V=O repulsion which becomes very strong in the δ-phase because of pronounced layer puckering.

It has been previously reported that for Li concentration $x = 1$, the δ-phase transforms into the ε-LiV_2O_5 phase at about 120 °C, after what around 350 °C the ε-phase converts into the γ-LiV_2O_5 phase [8]. The evolution of the Raman spectrum of δ-LiV_2O_5 heat-treated at different temperatures in the 100–250 °C temperature range is reported in Fig. 2. Besides the emergence of high-frequency bands, other characteristic

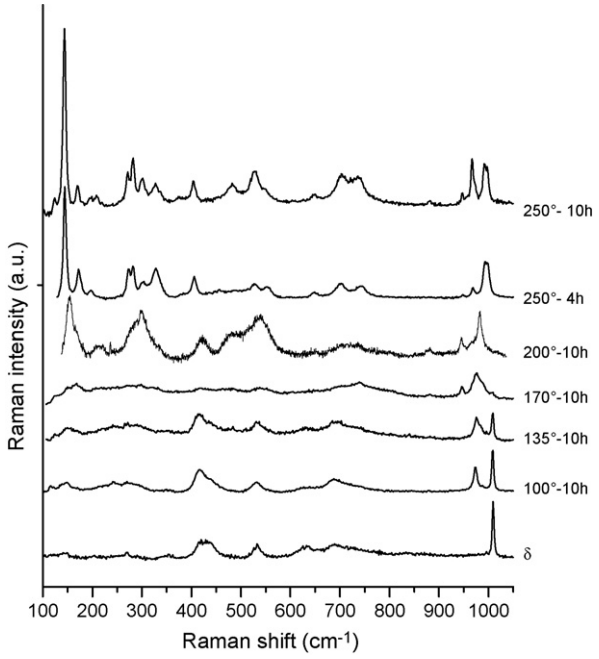

Fig. 2. Raman spectra of heat-treated δ-LiV_2O_5 at different temperatures.

frequency lines located in the 100–800 cm^{-1} range gradually appear, located at 145 cm^{-1}, 171 cm^{-1}, 271 cm^{-1}, 282 cm^{-1}, 301 cm^{-1}, 327 cm^{-1}, 404 cm^{-1}, 482 cm^{-1}, 528 cm^{-1}, 647 cm^{-1}, 703 cm^{-1} and 737 cm^{-1}.

Such strong spectral changes reveal the structural variation induced by the thermal treatment. The emergence of the high-frequency band at 975 cm^{-1} indicates that the δ → ε transformation begins from 100 °C. Up to 170 °C, both δ- and ε-phases coexist, the ε-phase growing at the expense of the δ-phase. At this temperature, the nucleation of the γ-phase begins, as pointed out by the appearance of a new feature at 945 cm^{-1}. At 200 °C, the Raman spectrum changes drastically with the emergence of intense and well-resolved Raman features in the whole wavenumber range indicating the crystallization of the γ-LiV_2O_5 phase. The ε → γ transformation ends at 250 °C, as shown by the disappearance of the 985 cm^{-1} band.

Hence the thermal treatment of the δ-phase at 250 °C allows to obtain the pure γ-phase LiV_2O_5 (space group *Pnma* or D_{2h}^{16}) with the following lattice parameters $a = 9.69$ Å, $b = 3.60$ Å and $c = 10.67$ Å. Such values are in good agreement with the structural data previously reported for γ-LiV_2O_5 [6,8]. The Raman wavenumbers of the different phases here synthesized are summarized in Table 1.

It comes out that all main spectral features observed in α-V_2O_5 can be clearly discriminated in the spectrum of γ-LiV_2O_5. Second, some bands which have a singlet form in the Raman spectrum of α-, ε- and δ-V_2O_5 are clearly twofold split in the spectrum of γth-LiV_2O_5. Third, some new spectral features not seen in the Raman spectrum of α-V_2O_5 can be detected in the spectrum of γ-LiV_2O_5 (bands at 376 cm^{-1}, 546 cm^{-1}, 647 cm^{-1} and 966 cm^{-1}). At least two factors can account for the distinction between the spectra of these crystals. First, the non-equivalent character of the ladders in the lattice of γ-LiV_2O_5, inducing two kinds of vanadium environments, must lead to the twofold splitting. Second, the Li atom oscillations may couple with some modes of the V_2O_5 lattice. Our lattice dynamics calculations actually in progress confirm this suggestion, especially for the high-frequency modes.

Table 1
Wavenumbers (in cm^{-1}) of Raman active modes observed for the α, ε, δ and γ phases of $Li_xV_2O_5$ samples

α-V_2O_5	ε-$Li_{0.52}V_2O_5$	δ-LiV_2O_5	γ-LiV_2O_5
145	154 s	145 vw	145
196	218 w		171, 197
			209
283	284 m	271 vw	271, 282
304	300 m	355 vw	301, 327
	420 s	420 s	376
404	486 w	435 s	404
480	535 m	533 s	482
526		630 m	528
	703 s	690 m	546
		837 vw	647
697	983 s	1008 vs	703, 737
			881
			947
			966
994			992, 997

vs, very strong; s, strong; m, medium; w, weak; vw, very weak.

In other respects, we show that the δ-LiV_2O_5 compound is very sensitive to the power of the incident radiation. Indeed, the use of a laser power higher than 200 μW provokes the *in situ* transformation of the δ-phase into the γ-phase (Fig. 3). This metastable character of the δ-phase allows explaining the great disparities encountered in the literature spectra. It is worth mentioning that the Raman spectrum reported by Zhang and Frech [13] as corresponding to that of δ-$Li_{0.95}V_2O_5$ exhibits striking similarity with that of the laser induced γ-LiV_2O_5 form (Fig. 3e).

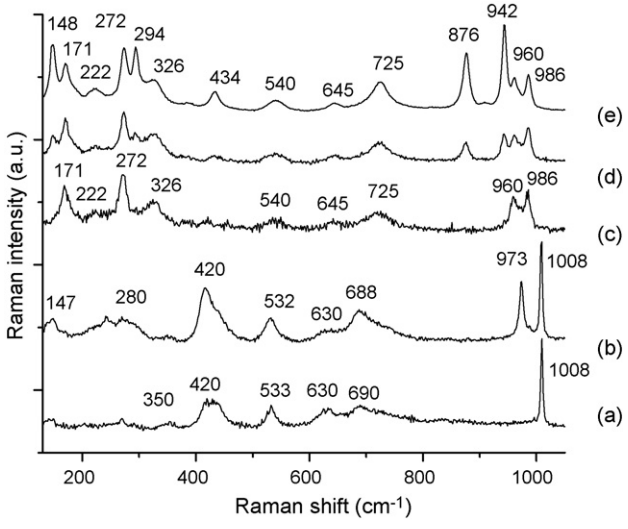

Fig. 3. Raman spectra of chemically δ-LiV_2O_5 powder illuminated with laser power of 0.2 mW (a) laser power of 0.6 mW (b) laser power of 0.8 mW, integration time: 20 s (c) laser power of 0.8 mW, integration time: 90 s (d) laser power of 0.8 mW, integration time: 900 s (e).

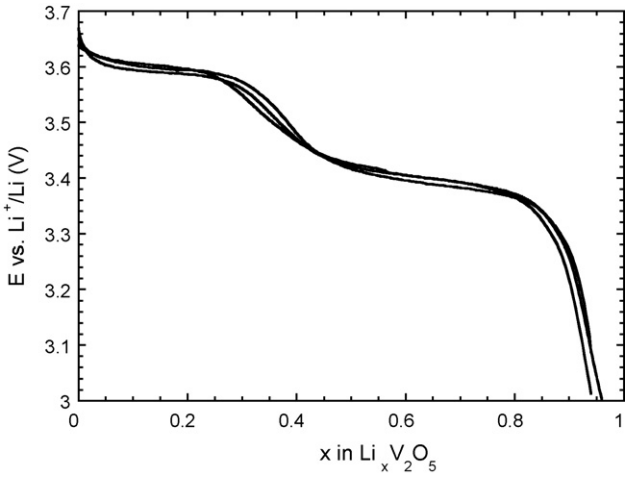

Fig. 4. Typical discharge–charge profile for a thin film V_2O_5 electrode (C/5 rate).

3.2. *In situ* Raman study of lithium insertion–extraction in V_2O_5 films prepared by dc sputtering

In this part, *in situ* Raman microspectrometry has allowed to get a dynamic picture of the cathodic material under operation. The discharge–charge curves of the thin film V_2O_5 electrode (Fig. 4) correspond to the typical well-known profile observed for bulk V_2O_5.

The evolution of the Raman spectra recorded during the first discharge of the thin film V_2O_5 electrode (Fig. 5) clearly shows that the whole spectrum is altered by Li insertion.

A more careful examination leads to the following comments: (i) from the first lithium contents, we observe a continuous intensity decrease of the low-frequency mode which indicates a progressive increase of the disorder in the plane of the sheets. (ii) Up to 1 Li/mol, the observed spectra correspond to the fingerprint of the ε-phase reported in Fig. 1b, although it is possible to still observe the high-frequency line of the pure V_2O_5 material up to 0.4 Li/mol due to its high Raman activity.

It comes out that the Raman spectra can be safely assigned to the ε-phase in the entire $0 < x < 1$ composition range.

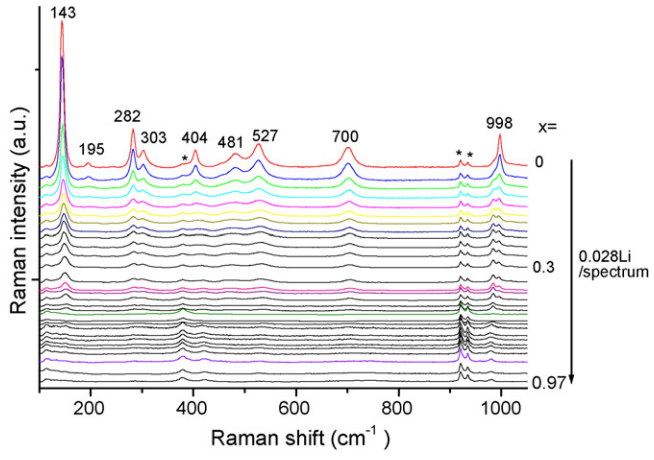

Fig. 5. *In situ* Raman spectra recorded during the first discharge of a thin film V_2O_5 electrode.

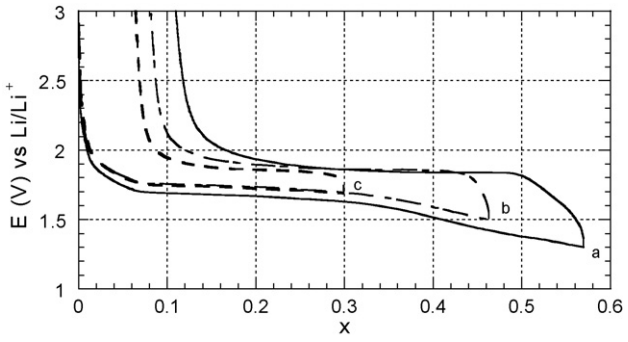

Fig. 6. Chronopotentiometric behaviour of anatase TiO_2 as a function of the depth of discharge in 1 M $LiClO_4$/PC (C/20); (a) $x = 0.56$; (b) $x = 0.45$; (c) $x = 0.3$.

It must be noticed that the V=O stretching frequency shows a continuous shift from 987 cm^{-1} to 980 cm^{-1} as lithium insertion proceeds. The related weakening of the vanadyl bond in the ε-phase can be related to XRD data, showing the existence a single phase behaviour in the $0 < x \leq 1$ lithium content range with a continuous shift of the main diffraction lines linked to an increase of the interlayer parameter from 4.4 Å to 4.65 Å. Moreover, the whole Raman spectrum of V_2O_5 is recovered after the reoxidation process, which indicates the structural reversibility of the lithium insertion in the $0 < x \leq 1$ lithium content range.

Hence the structural response of crystalline V_2O_5 thin films prepared by dc sputtering differs from that known for bulk powders. Surprisingly, a ε-related phase has been shown to exist in a wide composition range $0.3 < x \leq 1$ and the δ-phase has not been detected. Instead of that, an ε-solid solution seems to prevail in a wide composition range. Moreover, the γ-phase is never found for higher lithium contents.

3.3. *The Li/TiO_2 system*

TiO_2 anatase has a tetragonal symmetry (space group D_{4h}^{19}, *I*41*/amd*, number 141). The unit cell parameters are $a = b = 3.8$ Å; $c = 9.61$ Å. The typical chronopotentiometric behaviour of this compound is illustrated in Fig. 6.

At C/20 rate, one main discharge process located at 1.75 V is evidenced and corresponds to the insertion of 0.56 Li ion per mole of oxide. The charge process occurs at a higher voltage around 1.9 V with an efficiency (Q_{ox}/Q_{red}) around 80% showing the extraction of lithium ions from the cathodic material seems to be only partially quantitative whatever the depth of discharge is.

The chemical or electrochemical lithium insertion in the anatase structure is known to induce from the first lithium contents a phase transformation leading to lithiated titanate $Li_{0.5}TiO_2$ with orthorhombic symmetry (space group *Immm*) [3,14,15]. The Raman spectra obtained for the TiO_2 and $Li_{0.5}TiO_2$ compositions are shown in Fig. 7.

The five Raman bands at 144 cm^{-1}, 198 cm^{-1}, 398 cm^{-1}, 518 cm^{-1} and 639 cm^{-1} observed for the sample heat-treated at 400 °C for 5 h are typical of the anatase Raman fingerprint at room temperature. However, Raman data upon lithium insertion allow to evidence for the first time the vibrational fingerprint

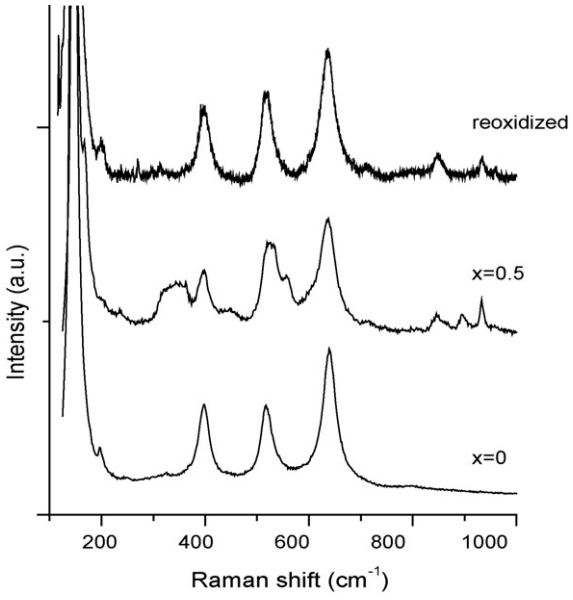

Fig. 7. Raman spectra for TiO_2, electrochemically (LT) $Li_{0.5}TiO_2$ and the reoxidized electrode.

of the (LT) phase, which exhibits several characteristic features. The main bands of pure anatase at 144 cm^{-1}, 398 cm^{-1}, 518 cm^{-1} and 639 cm^{-1} are kept. However new features are also observed, which consist in a complex band structure in the high wavenumber region, around 850 cm^{-1}, 900 cm^{-1} and 935 cm^{-1}, and two bands at 559 cm^{-1} and 166 cm^{-1}. Such changes in the Raman spectrum originate from the coupling between TiO_2 lattice modes and vibrations of the Li atoms, as shown from lattice dynamics simulation [16] based on the force constants transferred from other well-studied Li oxide compounds, and justified by the quantum mechanical simulations. This theoretical analysis has enabled us to predict the whole spectrum of Li-phonons and their interaction with TiO_2 lattice vibrations.

It comes out that the simulated Raman features corresponding to the orthorhombic Li-rich LT phase are in a good qualitative agreement with the reported Raman experimental spectrum. The complex structure of the observed Raman spectra is explained by multiplicity of the Li atom positions, which results in multiple Raman bands originated from the Li atom vibrations. Starting from the recent finding of multiple Li positions with rather anisotropic environment, and the suggestion of a short Li–O bond of 1.67 Å [17], lattice dynamics simulations show that lithium modes cover a wide frequency interval from 450 cm^{-1} up to 950 cm^{-1}, the high wavenumber Raman bands in the 900–950 cm^{-1} range being assigned to the stretching motion of rather short covalent Li–O bonds.

The Raman spectrum of the reoxidized material (Fig. 7) is typical of the anatase fingerprint. This indicates the restoration of the tetragonal TiO_2 framework upon oxidation. However the complex Raman band structure in the high-frequency region is still observed. These data suggest the presence of some covalent Li–O bonds which are not broken on reoxidation, and which are probably responsible for the partial loss of rechargeability of the material.

References

[1] D.W. Murphy, P.A. Christian, F.J. Disalvo, J.V. Waszczak, Inorg. Chem. 18 (1979) 2800.
[2] C. Navone, R. Baddour-Hadjean, J.P. Pereira-Ramos, R. Salot, J. Electrochem. Soc. 152 (9) (2005) 1790.
[3] R. Baddour-Hadjean, S. Bach, M. Smirnov, J.P. Pereira-Ramos, J. Raman Spectrosc. 35 (2004) 577.
[4] J.M. Cocciantelli, J.P. Doumerc, M. Pouchard, M. Broussely, J. Labat, J. Power Sources 34 (1991) 103.
[5] P.G. Dickens, S.J. French, A.T. Hight, M.F. Pye, Mater. Res. Bull. 14 (1979) 1295.
[6] J. Galy, J. Darriet, P. Hagenmuller, Rev. Chim. Min. 8 (1971) 509.
[7] P. Rozier, J.-M. Savariault, J. Galy, C. Marichal, J. Horschinger, P. Granger, Eur. J. Solid State Inorg. Chem. 33 (1996) 1.
[8] J. Galy, J. Solid State Chem. 100 (1992) 229.
[9] J.M. Cocciantelli, J.M. Gravereau, J.P. Doumerc, M. Pouchard, P. Hagenmuller, J. Solid State Chem. 93 (1991) 497.
[10] R. Enjalbert, J. Galy, Acta Cryst. C 42 (1986) 1467.
[11] L. Abello, E. Husson, Y. Repelin, G. Lucazeau, Spectrochim. Acta 39A (1983) 641.
[12] R. Baddour-Hadjean, V. Golabkan, J.P. Pereira-Ramos, A. Mantoux, D. Lincot, J. Raman Spectrosc. 33 (2002) 631.
[13] X. Zhang, R. Frech, Electrochim. Acta 42 (1997) 475.
[14] R.J. Cava, D.W. Murphy, S. Zahurak, A. Santoro, R.S. Roth, J. Solid State Chem. 53 (1984) 64.
[15] R. Van de Krol, A. Goossens, E.A. Meulenkamp, J. Electrochem. Soc. 146 (1999) 3150.
[16] M. Smirnov, R. Baddour-Hadjean, J. Chem. Phys. 121 (2004) 2348.
[17] M. Wagemaker, G.J. Kearley, A. van Well, H. Mutka, F.M. Mulder, J. Am. Chem. Soc. 125 (2003) 840.